

Wireless Laser Power Transmission: A Review of Recent Progress

Ke Jin , Member, IEEE, and Weiyang Zhou 

Abstract—Laser power transmission (LPT) is one of the most promising technologies in the long-range wireless power transfer field. LPT research has been driven by the desire to remotely power unmanned aerial vehicles, satellites, and other mobile electric facilities. However, the low overall efficiency is the main issue that limits the implement of high-intensity laser power beam (HILPB) system. As seen from the contemporary understanding of efficiency of laser power transmission channel, the efficiencies of laser and PV array are the main limiting factors to the HILPB system from the perspective of power conversion. Thus, a comprehensive overview of LPT technology is presented from the point of efficiency optimization view in this paper. First, the basic principles of laser power transmission are briefly summarized. Then, a survey of the efficiency optimization methods for HILPB system with regard to the laser and PV technologies is provided in detail. Additionally, the open issues and challenges in implementing the LPT technology are discussed.

Index Terms—Efficiency, Gaussian beam, laser, optical propagation, photovoltaic (PV), wireless power transmission.

I. INTRODUCTION

WIRELESS power transfer (WPT) is the technology that the electrical energy is transmitted from a power source to an electrical load without any electrical or physical connections. Compared to traditional power transfer with cord, WPT introduces many benefits such as better operational flexibility, user friendliness, and product durability. Therefore, WPT technology is ideal in applications where conventional conduction wires are prohibitively inconvenient, expensive, hazardous, or impossible [1]. Nowadays, the WPT technology is attracting more and more attention and evolving from theories toward commercial products, from low-power smartphones to high-power electric vehicles (EVs), and the wireless powered products will come to a 15 billion market by 2020 [2].

The development of WPT technology is advancing toward two major directions, i.e., near-field techniques, which have a typical transmission distance from a few millimeters to a few meters, and far-field techniques, where the coverage is greater

Manuscript received February 11, 2018; revised May 12, 2018; accepted June 20, 2018. Date of publication July 4, 2018; date of current version February 20, 2019. This work was supported in part by the National Natural Science Foundation of China under Grant 51377080, and in part by the Six Talents Peak Project of Jiangsu Province 2014-DZXX-017. Recommended for publication by Associate Editor C. T. Rim. (*Corresponding author: Ke Jin*)

The authors are with the Jiangsu Key-Laboratory of New Energy Generation and Power Conversion, College of Automation Engineering, Nanjing University of Aeronautics and Astronautics, Nanjing 210016, China (e-mail: jinke@nuaa.edu.cn; zhouweiyang@nuaa.edu.cn).

Color versions of one or more of the figures in this paper are available online at <http://ieeexplore.ieee.org>.

Digital Object Identifier 10.1109/TPEL.2018.2853156

or equal to a typical personal area network. The former consists of two techniques: Capacitive power transfer (CPT) [3] and inductive power transfer (IPT) [4], [5], while the latter can be further sorted into microwave power transfer (MPT) [6] and laser power transfer (LPT) [7]. The advantage, disadvantage, effective charging distance, and applications of these WPT technologies are highlighted as shown in Table I.

To date, both of the CPT and IPT can offer the capability of supporting high power transfer above kilowatt level with high efficiency in close distance [8], [9]. However, the transferred power of these technologies attenuates quickly with the increase in the transmission range. Thus, the power transfer distance is largely limited. Because of the ease and low cost of implementation, these near field WPT technologies have found niche applications in everyday life, such as wireless charging of consumer electronics, EVs, robot manipulation, and biomedical implanted devices.

With the near-field wireless power technology reaching a mature stage for domestic and industrial applications, far-field wireless power research has been gathering momentum in the last decade. Both the microwave and laser power transfers have the ability to transfer several kilowatts power over long distance up to several kilometers, which are more flexible than those near-field wireless power technologies. Despite the common advantage of long transmission range, the laser's efficient atmospheric propagation window and its ability to deliver large amounts of power to a small aperture separate it from the microwave technology and make it an enabling technology to extend the capabilities of existing applications and facilitate the development for completely new paradigms [10]. Benefits from the advancement of the laser and PV technologies, nowadays, the high-intensity laser power beaming (HILPB) system has the capability to deliver energy indefinitely to remote mobile electronic devices, such as unmanned aerial vehicles (UAVs) [10], robots [11], and orbiting satellites [12]. Moreover, it is considered to have the potential to connect lunar habitats, landing sites, and power plant, and can be easily reconfigured to serve as a flexible virtual power grid [13]. The vast application potential makes the pursuit of the HILPB system a worthwhile endeavor so that the full potential of the WPT will be realized in the near future.

The concept of LPT technology is based on the principle of photoelectric effect was proposed in 1965 [14]. However, the development of a practical HILPB system was slow at that time due to the low efficiencies of the system components. It was until the 2000s, a variety of valued research works and applications for LPT technology had been identified and assessed. One such work was the demonstration of laser-powered

TABLE I
CLASSIFICATION OF WPT TECHNOLOGIES

WPT technologies		Key advantages	Potential disadvantages
Near field	CPT	<ul style="list-style-type: none"> • High power transfer up to several kilowatts • Transfer power through metal objects without generating significant eddy currents losses • Use metal plates to transfer power, which can reduce the cost • Suitable for small size applications, but also can be used in large size applications, such as EV 	<ul style="list-style-type: none"> • Limited efficiency at the range of 70%-80%, though it can reach 90% in some applications • Short transmission distance, which is usually within the hundreds of mm range • The challenge comes from the conflict among the transfer distance and power as well as the capacitance value
	IPT	<ul style="list-style-type: none"> • High efficiency, which higher than 90% is possible • High power transfer up to several kilowatts • Good galvanic isolation • Suitable for applications that from low power smartphones to high power EV 	<ul style="list-style-type: none"> • Limited transmission distance, which vary from cm to m • The significant eddy current loss is generated in nearby metals which limits its application area
Far field	MPT	<ul style="list-style-type: none"> • Long effective transmission distance up to several km • Suitable for mobile applications • Potential to transfer several kilowatts power 	<ul style="list-style-type: none"> • Low efficiency less than 10% for high power applications (such as transfer several kilowatts power or more) • Complex implementation
	LPT	<ul style="list-style-type: none"> • Long effective transmission distance up to several km • Flexible device, suitable for mobile applications • Potential to transfer several kilowatts power 	<ul style="list-style-type: none"> • Low efficiency around 20% or less • Line-of-sight to the receiver

minirover conducted by EADS Space Transportation facility in 2002 [15]. This is considered as a first step toward the use of LPT technology for powering mobile electric devices. The demonstration was based on an Nd:YAG laser at 532 nm with an output power of 5 W, and the power required by the rover was about 1 W. A tracking system was developed to maintain an orthogonal angle between the PV cell panel and the laser beam over a distance up to 280 m.

Later on, the first successful demonstration of laser powered aircraft flight was performed by NASA in 2003 [10]. The aircraft was fitted with a custom thin-film PV array, and an adjustable 1.5-kW diode array at 940 nm with 50% efficiency was chosen. The 500-W laser power beam manually tracked the aircraft's flight path at 15 m range, resulting in a laser power of 40 W to the PV array and 7 W of power to the motor to sustain flight for 15 min. In this experiment, the beam spot size was rather large compared with that of the PV array and was thought the main factor limiting the power transmission efficiency rather than the losses in the laser and PV cells.

Then, in 2006, the Kinki University had successfully applied the LPT technology to the small aircraft [11]. The laser power of 300 W from a laser diode transmitter was used and the power converted by the 25% efficient GaAs PV array was about 40 W. The long time flight of the aircraft flying at an altitude of 50 m for more than 1 h with autotracking system had been demonstrated, which validated the feasibility of lase power transmission to an aircraft for a long time.

After that, LaserMotive, Inc., further advanced the LPT technology by demonstrating an HILPB system to power a robotic climber to a height of 1 km in 2009 NASA Centennial Challenges [16]. It was confirmed that over 1-kW optical power was transferred to a receiver with the overall efficiency more than 10%. In 2012, Lockheed Martin and LaserMotive, Inc., had conducted a series of proof-of-concept tests on the Stalker UAV to further validate the performance of an innovative laser power system. The demonstrations showed that the flight time of Stalker could be increased by 24 times using the laser power system. Although LaserMotive, Inc., has made great progress in

the field of LPT technology, relevant technical details have not been published yet [17].

Recently, Beijing Institute of Technology had demonstrated a laser power transmission system at 100 m based on an optimized photovoltaic (PV) converter in 2014 [18]. The system output power was 9.7 W and the overall efficiency was 11.6%. In addition, in 2016, Russia's Rocket and Space Corporation had successfully charged a cell phone across 1.5 km using a laser and a 60% efficient photoelectric converter. Such LPT technology will be applied to supply fuel to state-of-the-art satellites and military vehicles according to the Russian Academy of Cosmonautics [19].

Besides the above mentioned demonstrations of HILPB systems, some other validation HILPB systems also have been summarized in Table II. As seen in Table II, the LPT technology is still under development, most of the HILPB systems only can transmit several tens of watts across several hundred meters with relatively low efficiency and is far from its practical implementation. In order for the HILPB system to become a viable option for practical wireless power transfer, each component of the system must ensure sufficient high efficiency to provide for a high end-to-end system efficiency. Thus, most existing literatures presented relevant research works on LPT technology mainly from the perspective of device-level techniques and hardware implementations. In [22]–[24], the candidate laser technologies for laser power transmission are summarized from the aspect of power level, wavelength, and electro-optical efficiency. Works in [16], [25], and [26] focused on the performance of the PV receiver of the HILPB system. In order to achieve high-optical-electro efficiency under HILPB conditions, different types of PV cells and array structures are investigated. Motivated by the numerous publications in the field of HILPB technology and by an immense amount of their real-world residential and industrial deployments, the main aim of this paper is to provide a comprehensive survey of the HILPB system with regard to the laser and PV technologies from the efficiency point of view.

In this paper, a typical configuration of the HILPB system is presented and the basic principles of laser power transmission

TABLE II
SUMMARY OF MAIN COMPONENTS OF VARIOUS HILPB SYSTEMS

Literature	Laser Transmitter			PV Receiver				Whole System		
	Laser Type	Wavelength (nm)	η_{laser} (%)	Cell Type	η_{pv_cell} (%)	Incident energy (W/m ²)	η_{pv_array} (%)	Distance (m)	Output Power (W)	η_{system} (%)
[10]	Diode 1.5kW	940	50	Si	14.6	560	17	15	—	<8.5
[11]	Diode 400W	808	—	GaAs	—	300W	14	50	40	<14
[15]	Nd:YAG laser	523	—	InGaP	—	<5W	40	280	>1	—
[16]	Disk 8kW	1060	25	Si	35	2kW	5	10 ³	100	1.25
[18]	Diode 25W	793	30	GaAs	—	6×10 ⁴	40.4	100	9.7	11.6
[20]	Diode 2kW	810	—	GaAs	50	3×10 ³	21.9	100	200	—
[21]	Nd:YAG laser	1060	—	Si	50	300	14	3	19	<14

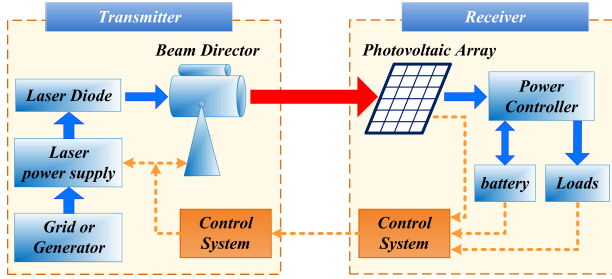


Fig. 1. Schematic diagram of a HILPB system.

are briefly summarized in Section II. Then, in Section III, the present enabling technologies for HILPB are provided, in order to make the best use of laser and PV array in the system, so that the system efficiency can be further improved. First, the current status of laser technology for high-power long-distance laser transmission is described from the perspective of power conversion. Furthermore, the efficiency optimization methods for PV receiver under Gaussian laser beam condition are introduced. Finally, an overview of future research trends and concluding remarks can be found in Sections IV and V, respectively.

II. BASIC PRINCIPLES OF LASER POWER TRANSMISSION

A. HILPB System Architecture

Fig. 1 schematically shows a block diagram of the HILPB system [10]. As seen, the transmitter of the system converts power from a common source (battery, generator, or grid) into a monochromatic beam of light via a laser. This laser beam is then shaped with a set of optics, and directed via a beam director to the remote PV receiver. While in the receiver, specialized PV cells matched to the laser wavelength and beam intensity convert the laser light back into electricity to be used to charge a battery, run a motor, or do other work. In many ways, the HILPB system can be viewed as a kind of extension cord, with electrical power

going in at one end, and electrical power coming out at the other end.

Ideally, an HILPB system would have the ability to transmit any amount of power to any point in space, but practical limitations such as conversion efficiencies at the source and the receiver limit the performance of an implemented system [10]. Therefore, the end-to-end system efficiency must be considered in order to make a fair assessment, when considering the feasibility of a HILPB system in a particular application. Since each component contributes to the overall system efficiency, the use of high performance components is fundamental in developing a successful system.

B. Available Types of Laser

Nowadays, there are various types of lasers. In principle, the selection of a laser for the HILPB system needs to comply with several fundamental constraints related to the: 1) the possibility to transfer the energy through the atmosphere; and 2) the possibility to transfer the energy as long as possible.

For the former constraint, as the atmosphere is comprised of various gases that fluctuate in composition due to environmental conditions, the atmosphere will absorb certain energies at particular wavelength. Thus, the lasers need to be considered must operate in the wavelength range centered around the spectrum in which the atmosphere is nearly transparent in order to maximize energy transfer. Fig. 2 shows the region of the atmospheric transmission spectrum within 15 μm . As shown in Fig. 2, although the atmosphere is relatively transparent in the region of 3–4 and 8–14 μm , the efficiencies of the corresponding lasers are relatively low. It is reported that the window in the region between 780 and 1100 nm is particularly relevant for commonly available laser technologies that produce sufficient power for wireless power transmission [24].

For the latter constraint, the other factor needs to be considered for selecting the available lasers is that the beam of the laser should be bright enough to ensure the energy can be transferred over a long enough range. The flux Φ delivered to the receiver

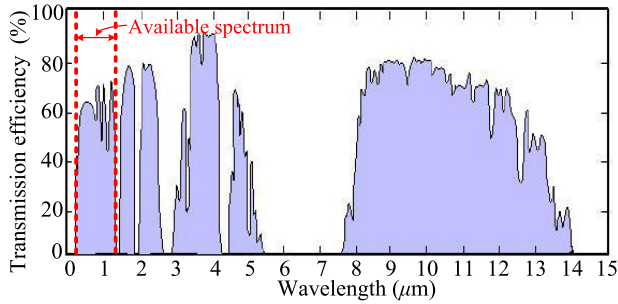


Fig. 2. Atmospheric transmission spectrum.

TABLE III
CURRENTLY AVAILABLE LASER TECHNOLOGIES

Laser Type	Wavelength λ (nm)	Efficiency η (%)	Radiance, R_{source} (W/m ² ·sr)
Diode, 10 kW	850	50	1×10^{10}
Thin disk, 25 kW	1060	25	2.4×10^{15}
Fiber, 10 kW	1060	25	4×10^{13}
Fiber, 20 kW	1060	25	1.4×10^{13}

at slant range L is given by [27]

$$\phi = \frac{R_{\text{source}} A_{\text{source}} \eta_{\text{trans}}}{L^2} \quad (1)$$

where R_{source} is the radiance (power per unit area per steradian) of the laser source, a constant that indicates the beam quality and cannot be changed by passive optics, A_{source} is the total area of the beam source, possibly spread across more than one telescope aperture, and η_{trans} is the transmission efficiency through the atmosphere.

From (1), in the condition that the flux Φ is given, the transmission range L is limited primarily by the source irradiance R_{source} and source aperture size A_{source} . This constrains the types of laser that could supply adequate radiance R_{source} .

As stated above, various types of lasers that could be considered candidates for beaming tens of kilowatts are listed in Table III [27]. As shown in Table III, the diode-pumped solid-state lasers (DPSSLs) such as fiber and disk lasers have the advantages of high power and good beam quality, which are suitable for high-power long-range HILPB systems. However, the relatively low efficiency limits the implement of the HILPB system in large-scale applications. Alternatively, the high-power LDs are more efficient, compact, and inexpensive than DPSSLs. While the LDs are not bright enough for long-range power transmission, so that the LDs are suitable for some low-power or short-range applications as most demonstrations of the HILPB system do so far. Nevertheless, with the development of the technology of the laser diodes, the high-power laser diodes would open up potential large-scale LPT applications.

C. Available Types of PV Cells

At the receiver of the HILPB system, the appropriate PV cell should be carefully designed so that the laser power can be effectively converted into electricity. In order to do so, the

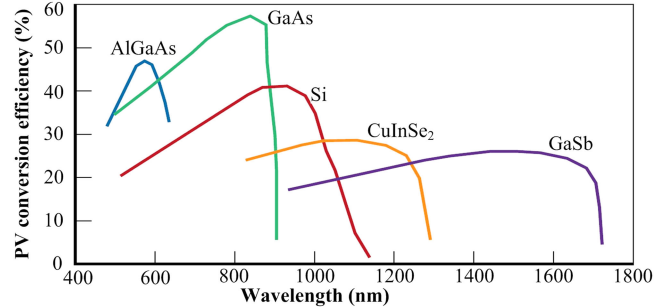


Fig. 3. Spectral response of some PV materials.

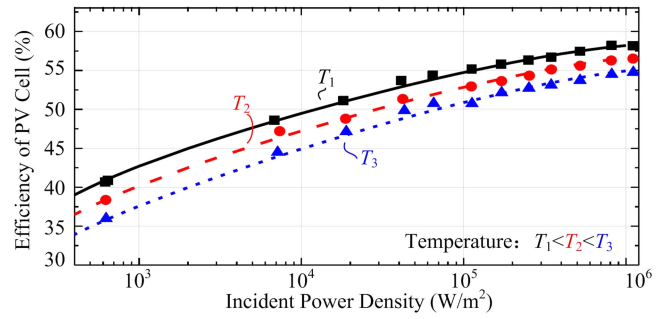


Fig. 4. Efficiency of the PV cell as a function of the incident power density.

factors of the laser power, wavelength, temperature, and the material of the PV cells should be considered.

For a PV cell, the photons must have energy greater than or equal to the band-gap in the material in order for the cell to generate electricity. Since the energy of a photon is proportional to its frequency, PV cells are responsive to particular frequencies of light corresponding to the cell's band-gap energies. Thus, the ideal light source would be monochromatic and at an ideal frequency for the PV material, instead of spread across a broad spectrum of frequencies, as sunlight is. The spectral-response curves for some different PV materials are illustrated in Fig. 3 [27]. As seen, the most widely used PV cells like Si and GaAs could reach the highest conversion efficiencies when illuminated with monochromatic beams of wavelengths 900 nm and 850 nm, respectively.

On the other hand, it is the fact that when a PV cell is illuminated with more intense light than the solar radiation, the cell not only generates more absolute power, it is also more efficient for a given temperature, as illustrated in Fig. 4 [28]. Thus, the PV cell that can provide efficient operation at high laser power intensity is more desirable.

Table IV shows estimated efficiencies under laser illumination for different PV materials. As seen from Table IV, the GaAs PV cell is the highest efficient PV converter. The GaAs PV cell has greater than 50% efficiency under light of the right wavelength [29]–[31]. Moreover, the GaAs PV cell is best suited to wavelengths around 850 nm, which is ideal for the LDs. While, for Si PV cell, the most ideal wavelengths comes at about 900–950 nm, but atmospheric absorption is too high in this region to make Si PV cells a strong competitor [27]. The InGaAs, InGaP, and CIS cells are responsive to the wavelengths of more than 1 μm , which are ideal for the DPSSLs. However,

TABLE IV
EFFICIENCIES OF DIFFERENT PV MATERIALS UNDER LASER ILLUMINATION

PV Material	GaAs		Si		InGaAs/InP	InGaP	CIS
Suitable Laser Wavelength	810nm		950nm		>1000nm		
$\eta_{pv}(\%)$	53.4	60	27.7	28	40.6	40	19.7
Incident laser intensity (kW/m ²)	430	110	10	110	2.37	2.6	10

TABLE V
COMPARISON OF SOME POSSIBLE LASER AND THEIR MATCHED PV CELL

Available Commercial Laser	Wave-length λ (nm)	η_{laser} (%)	Suitable PV Material	η_{pv} (%)	Theoretical Transmission Distance
Diode, 10 kW	850	50	GaAs	>50	<10km
Fiber, 20 kW	1060	25	CIS	17	<100km

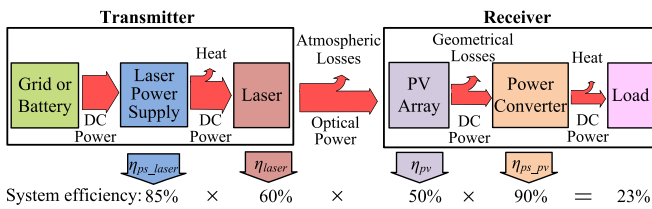


Fig. 5. Ideal efficiency of a HILPB system.

these materials are not efficient enough under high illumination intensity [15], [27].

D. Ideal Efficiency of HILPB System

Above all, a comparison of some possible laser and their matched PV cell options is shown in Table V. Note that this table, although the fiber laser offers the benefits of higher power level and longer transmission distance, also brings challenges that arise from the lower efficiency and the higher cost. On the contrary, although the LD is still not bright enough to ensure long enough transmission distance for a practical HILPB system, it has shown significant efficiency improvements as well as its matched GaAs PV cell does. Thus, the LD and GaAs PV cell tend to be the best option for the HILPB system.

Fig. 5 shows the flow of power from input to output and the contemporary understanding of efficiency of each component in the HILPB system [10], [32], [33]. Currently, the commercial off-the-shelf LD can offer high efficiency of 40–60% with laser power around 1 kW [34]. However, when the output power is more than hundred watts, the dissipated heat is quite large and the cooling system is complex. More increase in the efficiency of laser is strongly required. Current specialized GaAs PV cells designed for high-intensity laser energy applications (intensities 500 times of the sun or greater) can achieve more than 50% optical-electro efficiency [28]. However, the efficiency of the PV array is roughly 30–40% or even lower [32]. This is mainly because of the nonuniform beam distribution so that all the cells cannot receive the laser light at the optimum operation condition. On the other hand, the atmospheric scattering and absorption can also degrade the performance of the system, and

the highest transmission efficiency of the laser through the atmospheric is around 80%, as shown in Fig. 2. Thus, for the system, the currently possible maximum overall efficiency of the system is only about 23% in theory, as seen in Fig. 5, regardless of the disturbances in the transmission medium. As the laser and PV technologies evolve, it is expected that the overall system efficiency could exceed 30%, and eventually approaching 50% [35].

As shown in Fig. 5, although there have been many recent advances in the field of laser and PV technologies, the main limiting factors to the HILPB system are the efficiencies of the laser and PV receiver. Hence, as shown in Table I, the operation efficiency of the system is only around 10% in practice, which is much less than the ideal efficiency of the system. It is indicated that there is a much room to improve the operation efficiency of the system. Besides the requirement for improving the theoretical maximum system efficiency by developing new materials and structures for lasers and PV cells, some limitations in the practical application, such as the effect of Gaussian laser beam to the efficiency of PV receiver, should be carefully considered from the perspective of power conversion; thereby, the ability of the laser and PV array can be fully used and the operation efficiency of the system can be improved as close to its theoretical maximum efficiency as possible. It can be foreseen that the continually being improved WPT technologies will generate an opportunity to allow the HILPB systems have greater power handling capacities and conversion efficiencies. Therefore, the HILPB systems can be used to charge the mobile electronic devices due to its flexibility. Moreover, benefits from the characteristics of laser, the HILPB systems is suitable for delivering power to electronic devices in high voltage, RF, EMI, and magnetic fields.

III. ENABLING TECHNOLOGIES FOR HILPB

As mentioned above, the efficiencies of the laser and PV array impose more severe effect on the performance of a HILPB system than that of power converters, so that improving their efficiency is strongly required. In this section, in order to make the best use of laser and PV array in the system, the methods that can be employed to optimize the efficiency of the laser and PV array are summarized from the perspective of power conversion.

A. Efficiency Optimization Method for LD

1) *Methods to Improve the Efficiency of the LD*: As mentioned above, the LD is a core component in the system. It is well known that the LD is a current driven device. Thus, the input current has an apparent effect on the output of the LD. The relationship between input current i and output optical power p_o

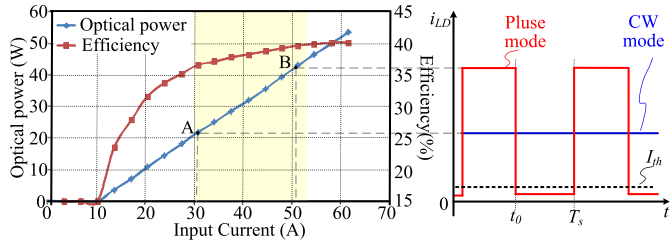


Fig. 6. Typical electrical characteristics of LD.

of an LD can be expressed by the following equation [36]:

$$p_o = \eta_d(i - I_{th}). \quad (2)$$

Here, η_d is the differential slope efficiency and I_{th} is the threshold current. For simplicity, both of them are supposed to be constant. As the voltage across the LD's terminals varies little with the change of the input current; thus, a constant value $V_{LD,in}$ can be used. The conversion efficiency η can be described by using

$$\eta = \frac{p_o}{p_{in}} = \frac{\eta_d(i - I_{th})}{V_{LD,in} \cdot i} = \frac{\eta_d}{V_{LD,in}} \left(1 - \frac{I_{th}}{i} \right) \quad (3)$$

where p_o is the input power of the LD. Fig. 6 shows the typical electrical characteristics of the LD. As can be seen, above threshold current, the optical power increases dramatically with the input current and keeps a linear relationship with the current. Furthermore, the conversion efficiency is increased along with the rising input current, and the growth rate of efficiency will slow down when input current comes to a certain extent if the temperature effect of the LD is ignored. In most practical WPT applications, the power rating of LD needs to be overdesigned to cope with atmospheric absorption. Hence, the LD does not have to keep running at full power all the time under rated condition (e.g., the operating region of the LD falls in the yellow areas of Fig. 6). This offers the advantages of lowering thermal stress to the LD and, thus, increasing lifetime, though the cost is increased.

In general, the LD can operate in a continuous wave (CW) mode or pulse mode for the purpose of wireless power transmission according to the types of the input current. As shown in Fig. 6, it is assumed that the point A is the operating point of LD in a CW mode. While, in order to output the same average optical power, the operating point of an LD in pulse mode can be located at point B during the interval $0 < t < t_0$. It is obvious that driving LD in pulse mode has a higher efficiency at this moment. However, during the interval $t_0 < t < T_s$, no light output in pulse mode and, thus, the efficiency of LD in pulse mode is lower than that in CW mode. Thus, it can be observed that with the same optical output power, the operating points of LD in different modes are different, and this could lead to the efficiency difference in different modes.

Based on the above observation, the study in [36] points out that driving LD with a pulse current gives better performance. Fig. 7 shows the experimental results of the variation of the LD efficiency in CW and pulse mode. Here, D is the duty cycle of the pulse laser and $D = 1$ represents CW laser. As shown, by the same output optical power, the smaller the duty cycle of the pulse laser, the higher efficiency will be achieved.

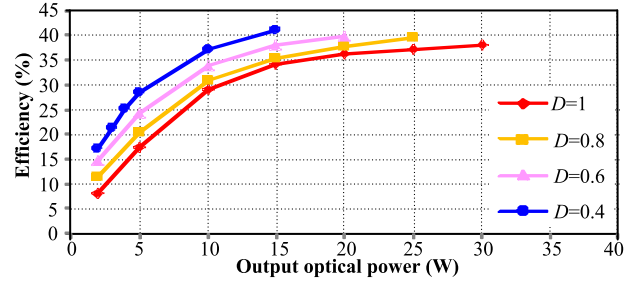


Fig. 7. Efficiency of the LD under CW and pulse mode.

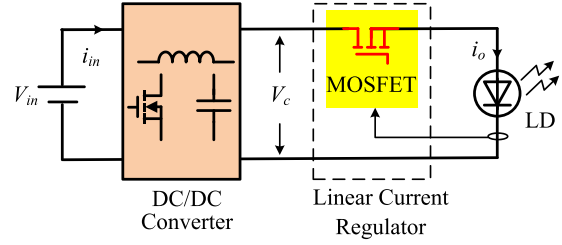


Fig. 8. Linear power supply for LD.

Thus, driving LD in a pulse mode is recommended and it can offer a chance to exploit the best performance of the LD. Moreover, it indicates that driving LD in pulse mode may give a chance for the system to further improve the operation efficiency in practice, if the whole system operates in a pulse mode. The more detailed analysis can be found in [36].

2) *LD Driver*: The LD driver is also a major component in the HILPB system, whose performance directly affects the output characteristics of LD. As well known, LD should be powered by a current source, and the main issue of the LD driver is to provide a driving current with extremely low ripple (usually lower than few tens of millamps) for the best light output performance.

In order to do so, the typical LD power supply usually consists of a linear current regulator, as shown in Fig. 8. However, the linear current regulator has such disadvantages as low efficiency and bulky volume in high power applications. The switching mode LD driver is an alternative to the traditional linear power supply. The switching mode LD driver based on a buck type converter with a high-order passive filter at output is the most common topology for generating current with a low ripple, as shown in Fig. 9 [37]. However, this approach has such disadvantages as it offers a heavy, bulky solution, and it leads to worse dynamic response. Another attractive option is to employ a typical interleaved multiphase buck converter [38]. However, the ability of the interleaved converter to cancel the current ripple depends on the duty cycle.

To further reduce the size and weight of the LD driver while maintaining low current ripple, some active ripple filter topologies have been proposed in [39] and [40]. In general, the active ripple filters have two types, which are feedforward filter and feedback filter. The feedforward filter achieves the ripple reduction by measuring a ripple component and injecting its inverse, as shown in Fig. 10(a). While the feedback filter, which is shown in Fig. 10(b), works by sensing the ripple current at the output

TABLE VI
PERFORMANCE COMPARISON OF THREE TYPES OF LD PULSED POWER SUPPLY

Type	Efficiency	Power density	Implementation complexity	Notes
DC/DC converter with linear regulator [41]	Low	Low	Medium	<ul style="list-style-type: none"> Fast rise/fall time of LD current No current overshoot Low current ripple
DC/DC converter with auxiliary converter [36]	Medium	High	Medium	<ul style="list-style-type: none"> Fast rise/fall time of LD current can be achieved if the bidirectional converter is carefully designed Current overshoot is existed Large current ripple
Single-stage converter [42]	High	Medium	Low	<ul style="list-style-type: none"> The rise/fall time of LD current is limited by the output filter Current overshoot is minimal owing to peak current control Low current ripple can be achieved owing to well-designed output filter

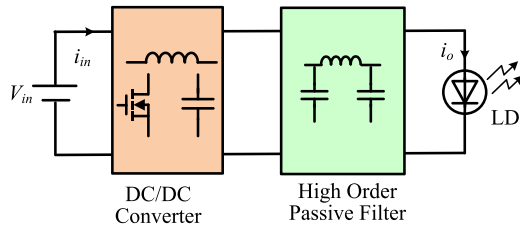


Fig. 9. Switching power supply for LD.

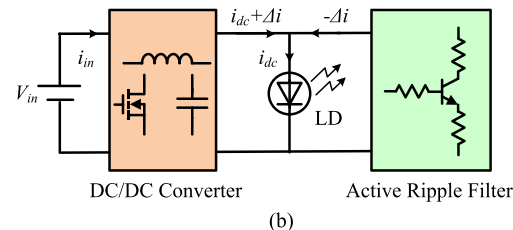
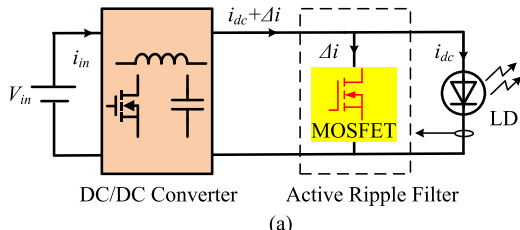


Fig. 10. Switching power supply with active ripple filter for LD. (a) LD driver proposed in [39]. (b) LD driver proposed in [40].

of the filter and driving it toward zero via high-gain feedback control.

As stated above, driving LD in the pulse mode gives a better performance, so that it is necessary to develop pulsed power supply for the LD. Here, three different types are discussed, and the performance comparison of these types is shown in Table VI.

In the first type, a buck converter in series with a high-speed switching transistor array Q is proposed to provide pulse current to LD, as shown in Fig. 11(a) [41]. The buck converter generates a dc current, and the transistor array Q switches the dc current to either LD or the shunt resistor. If the LD is ON, the dc current is sent to LD, otherwise, the dc current is sent to the shunt resistor and the input current of LD is zero. Although high dynamics is achieved, the power that is sent to the shunt resistor is sacrificed.

In the second type, a bidirectional converter is parallel to a dc–dc converter, which based on the concept of active power

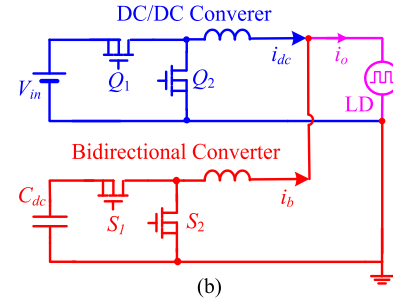
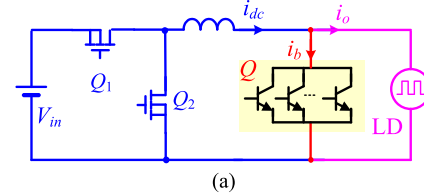


Fig. 11. Pulsed power supply for LD. (a) LD driver proposed in [41]. (b) LD driver proposed in [36].

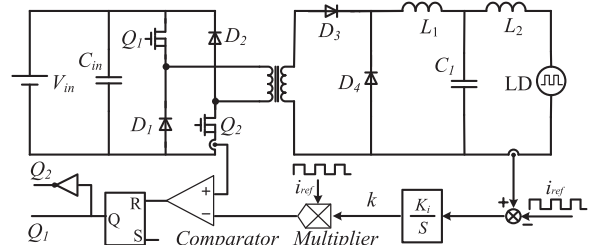


Fig. 12. Single-stage pulsed power supply for LD.

decoupling method, is proposed to provide pulse current for the LD [36]. As shown in Fig. 11(b), the dc–dc converter employs average current control, with the objective of providing the average output current to the LD during the operation. The bidirectional converter is employed as the storage unit to generate the ac component of the output current. As seen, the capacitor C_b of the bidirectional converter can be reduced by increasing the voltage on it. Thus, there exist theoretical possibilities to reduce the volume and weight of the storage capacitors and increase the power density.

In the third type, a single-stage pulsed power supply, which does not use any linear regulator, is proposed in [42]. Its circuit diagram is illustrated in Fig. 12. As seen, this pulsed power supply is based on a two-transistor forward converter, and a

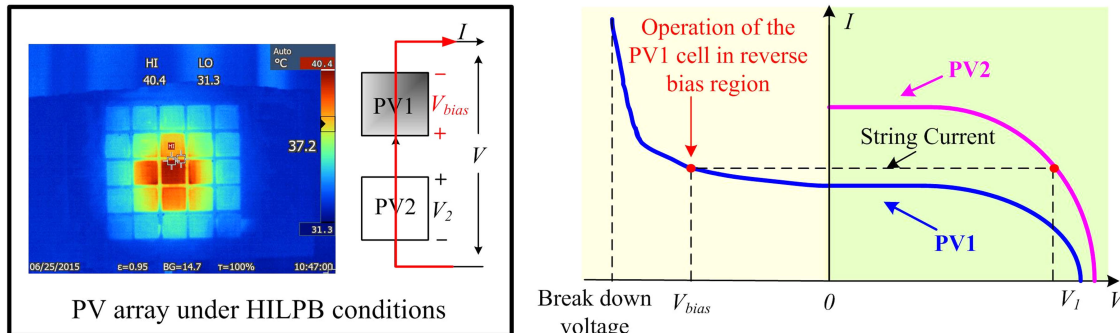


Fig. 13. Current–voltage curve of a PV cell operating in a reverse bias region.

third-order passive filter is used at the output of the converter to attenuate the ripple of LD current. The peak current control driven by a weighted pulsed reference is employed to control the converter. The weighting factor k is used to adjust the average value of pulsed LD current. Since linear regulator stages and/or auxiliary components are not included, high-power conversion efficiency is achieved.

B. Efficiency Optimization Method for PV Array

1) *Effects of the Gaussian Laser Beam:* In practice, the flat plate array is one of the most common PV receivers for the HILPB system. Since the Gaussian distribution of the laser beam, significant power losses would happen in the receiver. Thus, the efficiency of the PV array could be much less than that of a PV cell under Gaussian beam condition, as shown in Table I. It is indicated that the high-efficient PV cell cannot be fully used.

The key reason that causes the effects of the Gaussian laser beam is the current mismatch for each PV cell in a series string. Fig. 13 illustrates how the string current flows through all the series-connected cells under nonuniform illumination conditions [43]. The bias voltage V_{bias} is the reverse voltage at which the least illuminated cell must operate to support the common string current. Thus, the least illuminated cell consumes power due to the reverse voltage polarity, and the maximum extractable power from the PV receiver decreases. This, in turn, may cause the thermal break down of the cell, creating a so-called hot spot. This hot spot can be avoided by using the bypass diodes. These diodes are connected parallel to the cells to provide an alternate current path and, hence, limit the power loss in the least illuminated cells. However, the power-voltage (P - V) characteristics of the PV array get more complex with multiple peaks. The presence of multiple peaks reduces the effectiveness of the conventional MPPT technologies, and leading to the PV array becomes less efficient.

2) *Methods to Improve the Efficiency of the PV Array Under Gaussian Beam Condition:* To mitigate the effects of the nonuniform irradiance, there are four main approaches that have been proposed and these approaches can be employed to improve the efficiency of the PV array under Gaussian beam condition.

a) *Global MPPT techniques:* The first approach includes modified MPPT techniques that properly detect the global maximum power point (GMPP), and these global MPPT (GMPPT) techniques can be further categorized into three groups.

In the first group, several GMPPT methods are proposed including the diving rectangle (DIRECT) method [44], Fibonacci method [45], MPT method [46], and I - V curve approximation method [47]. In these methods, a relatively large voltage searching range is initially selected. Then, the searching range is gradually reduced until the GMPP is finally located. These techniques are relatively simple and easy to implement. They can fast track the GMPP with acceptable accuracy.

The DIRECT technique is basically a perturbation and observation (P&O) algorithm that its voltage search range is determined based on the Lipschitz condition of the function $p(v)$ which describes the relationship of the PV array power and voltage. For the uniformly bounded power function $p(v)$ on the voltage interval $[a, b]$, (4) is deduced

$$p(v) \leq \max(p(v)) \leq p(v_1) + M \frac{b - a}{2} \quad (4)$$

where v_1 is the sampling point which is at the center of $[a, b]$, v is a variable, and M is a Lipschitz constant. It can be seen that (4) gives a bound on how far the GMPP is deviated from the observed sample $p(v_1)$. Both M and $(b-a)$ might be large initially. However, by taking further iterations, the voltage searching range $(b-a)$ can be replaced by a smaller length of searching range successively. In each iteration, the voltage searching range $[a, b]$ is divided into three equal subintervals. Among which, the interval j is considered as the potentially optimal searching range if the following inequalities are satisfied:

$$p(v_j) + k \frac{b_j - a_j}{2} \geq p(v_i) + k \frac{b_i - a_i}{2}, \text{ for any } i \quad (5)$$

$$p(c_j) + k \frac{b_j - a_j}{2} \geq P_{\max} + \varepsilon |P_{\max}| \quad (6)$$

where P_{\max} is the current tracked maximum power, and ε as well as k is a positive constant value. a_i , b_i , a_j , and b_j are the end points of the i th and j th intervals, respectively. $P(c_i)$ is the sampling power taken at the center of the i th interval. The inequality (5) chooses the new searching range, which has the highest potential for the maximum power, for further exploration. The inequality (6) ensures that the new searching range would yield further improvement than P_{\max} by at least $\varepsilon |P_{\max}|$.

In [45], the Fibonacci search method, which is similar to the P&O method, is proposed. The Fibonacci search method iteratively restricts and shifts the searching range until the GMPP falls in the searching range. The process of restricting and shifting is illustrated in Fig. 14. First, the direction of the search

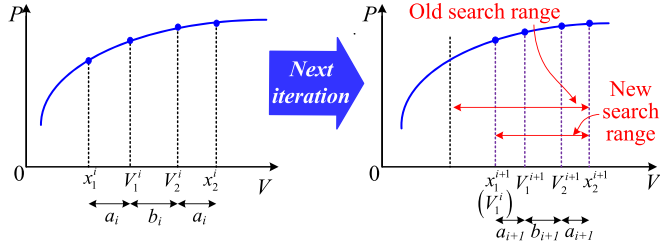
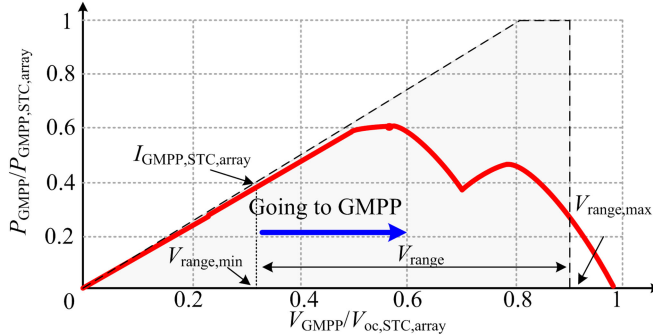


Fig. 14. Schematic diagram of the Fibonacci search method.

Fig. 15. MPT in the P - V plane.

shifting is decided based on the following rule:

$$\begin{cases} \text{if } p(v_1^i) < p(v_2^i), \text{ Then } [x_1^{i+1}, x_2^{i+1}] = [v_1^i, v_2^i] \\ \text{if } p(v_1^i) > p(v_2^i), \text{ Then } [x_1^{i+1}, x_2^{i+1}] = [x_1^i, v_2^i] \end{cases} \quad (7)$$

where x_1 and x_2 are the bounds of the searching range, v_1 and v_2 are the two check points in the range, the subscript i represents the iteration number, and $p(v_1^i)$ ($p(v_2^i)$) is the sampling voltage at the check point v_1 (v_2) in i th iteration. Then, in each iteration, the size of the searching range is determined by the Fibonacci sequence, such as

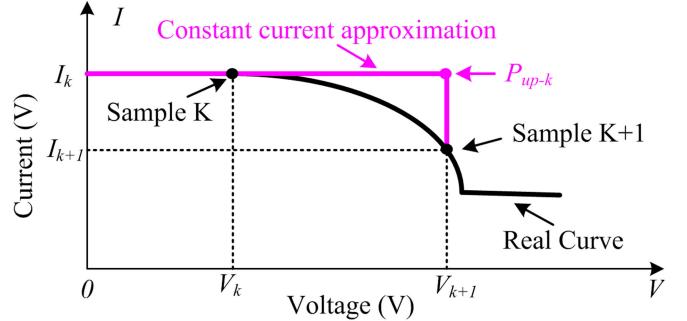
$$\begin{cases} \frac{a_i}{b_i} = \frac{c_{n+1}}{c_n} \\ \frac{a_{i+1}}{b_{i+1}} = \frac{c_n}{c_{n-1}} \end{cases} \quad (8)$$

where a_i represents the distance between the check point v_1 (v_2) and the interval bounds x_1 (x_2), b_i represents the distance between the two check points v_1 and v_2 and c_{n-1} , c_n , c_{n+1} are defined in the following manner:

$$\begin{cases} c_0 = 0, c_1 = 0 \\ c_n = c_{n-2} + c_{n-1}, n \geq 2. \end{cases} \quad (9)$$

As the experimental results shown in [45], the Fibonacci search method can quickly find the GMPP by doing a wide range search, but it may mistakenly detect the local maximum power point (LMPP) instead of the actual GMPP if there are many local MPPs in the P - V curve.

In [46], the MPT method is a modified P&O method which utilizes the knowledge of the MPT (a trapezoidal area in the P - V plane) to reduce the voltage searching range. It is reported that the trapezoidal area, as shown in Fig. 15, contains all possible GMPPs for any nonuniform irradiance conditions. As seen, the trapezoidal area is limited to the right by a vertical segment at $0.9 V_{oc,STC,array}$ and limited to the left by a segment in the origin with a slope of $I_{GMPP,STC,array}$ (array GMPP current at STC). During the process of tracking the GMPP, the upper bound of the

Fig. 16. Approximation of I - V curve.

voltage searching range is fixed at $V_{range,max} = 0.9 V_{oc,STC,array}$ (open-circuit voltage of the array at STC). The lower bound of the voltage searching range is determined by

$$V_{range,min} = \frac{P_{max}}{I_{GMPP,STC,array}} \quad (10)$$

where P_{max} is the current tracked maximum power. As seen, the lower bound $V_{range,min}$ increases along with the increase of the detected P_{max} . Therefore, since $V_{range,min}$ increases in each iteration and $V_{range,max}$ is fixed, the voltage searching range is gradually reduced until the GMPP is reached.

The I - V curve approximation method proposed in [47] can narrow the searching window and tracks the GMPP very fast. First, it takes some samples from the PV array and divides the voltage searching range into small subregions. Then, the method approximates the I - V curve in each subregion with a simple curve, as shown in Fig. 16. As seen, an upper limit P_{up-k} for the array power in subregion k [V_k , V_{k+1}] can be set as follows:

$$P_{up-k} = V_{k+1} \times I_k \quad (11)$$

where I_k is the current of the sample K . Obviously, the GMPP is not in that subregion whose upper limit P_{up-k} is lower than the maximum value of all measured powers P_{max} and this subregion can be eliminated from the searching range. Therefore, by comparing P_{max} with the estimated up limits, the searching range is limited. Hereafter, with similar procedure and further intelligent samplings, the searching range becomes smaller gradually until the vicinity of GMPP is achieved.

The second group is the GMPPT methods that utilize the unique characteristics of the I - V or P - V curves of the PV array under nonuniform irradiance conditions to track all the LMPPs or move operation point to the neighborhood of GMPP. Then, the conventional P&O or IncCond method can be adopted to attain the GMPP. Some examples of these methods are summarized as follows.

The load-line method, which is proposed in [48], utilizes the load line to bring the operating point into the vicinity of the global maximum. The function of the load line is defined as

$$I = \frac{I_{mpp}}{V_{mpp}} V = \frac{0.8V_{oc}}{0.9I_{sc}} V \quad (12)$$

where I_{mpp} , V_{mpp} , V_{oc} , and I_{sc} is the current of the MPP, voltage of the MPP, open-circuit voltage, and short-circuit current of the array under uniform irradiance conditions, respectively. When the nonuniform irradiance occurs, it is claimed that the operating point is moved to the neighborhood of the GMPP, which is the

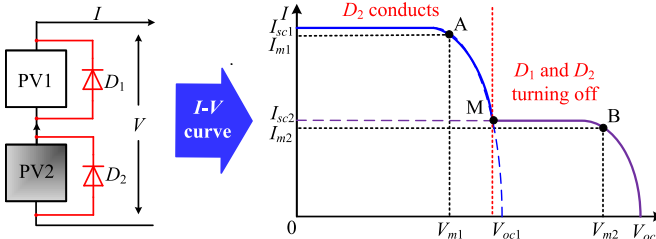


Fig. 17. Simple PV string under nonuniform illumination.

result of intersection of the load line with the I - V curve of the PV array. Then, the conventional MPPT methods, such as P&O method, are used to find the GMPP. It can be seen that the load-line method is simple and can achieve fast tracking speed, but the tracking result may be one of the local MPPs rather than the GMPP.

In order to improve the tracking accuracy, the power increment method is proposed in [49]. In this method, the searching process starts from the open-circuit condition, the power converter connected to the PV array is controlled as an adjustable power load and the power drawn from the PV array is increased at each step, resulting in the operation point moving toward the GMPP. Once the drawn power cannot be further increased, the power increment process is stopped and the power converter controls the operation point back to the last detected point. Therefore, the neighborhood of GMPP is determined. Then, the conventional MPPT methods can be adopted to attain the GMPP. As the experimental results shown in [49], the difference between the tracked GMPP and the actual GMPP is less than 0.1%. However, as the power increment method needs to search a large range of voltage, so that the tracking speed of the power increment method is slower than that of the load-line method.

In [50], a simple GMPPT method, referred to here as ramp voltage scanning method, is proposed. By observing the I - V and P - V characteristics of PV array, it is worth noting that the positions of all peaks in P - V curve (includes the GMPP of the array) stay at the following voltage range under nonuniform irradiance conditions:

$$V_{\text{mpp-mod}} < V < 0.9V_{\text{oc-arr}} \quad (13)$$

where $V_{\text{mpp-mod}}$ is the voltage of the module at its MPP and $V_{\text{oc-arr}}$ is the open-circuit voltage of the array under nonuniform irradiance conditions. To scan the restricted voltage range, this method uses the ramp voltage command (instead of conventional step-like changes) as the voltage reference of the converter connected to the PV array and simultaneous sampling the voltage and current of the array continuously. In this method, as the oscillation of array voltage can be avoided, the long delays in usual methods for correct sampling of voltage and current are not needed anymore. However, it searches almost all the range of P - V curves and, thus, its tracking speed is still not good enough.

The $0.8V_{\text{oc-mod}}$ model method, which is proposed in [51]–[54], is based on the conclusion that the peaks of a P - V curve under nonuniform irradiance conditions occur nearly at multiples of 80% of module's open-circuit voltage $V_{\text{oc-mod}}$. In [51], the proposed method first samples the P - V curve in distances of $0.8V_{\text{oc-mod}}$. Then, in the vicinity of each sample, the conventional P&O method is used to track the local peak in case of sign change of dP/dV . Finally, by comparing all peaks,

the GMPP is determined. Even though the $0.8V_{\text{oc-mod}}$ model method only needs to search the vicinity of the $0.8V_{\text{oc-mod}}$ regions rather than the entire P - V curve, the tracking speed of this method is generally slow for long PV string applications because each peak must be searched by the P&O method. On the other hand, Ahmad and Salam [52] point out that the peaks of P - V curve are located at the multiples of $0.8V_{\text{oc-mod}}$ which is not always true, especially for long PV strings. Therefore, the $0.8V_{\text{oc-mod}}$ model method may lead to incorrect GMPP detection. The further study about the $0.8V_{\text{oc-mod}}$ model method is presented in [53]. In [53], it is claimed that the value of the minimum voltage interval between the MPPs varies in a wide range starting from $0.5V_{\text{oc-mod}}$. Thus, the proposed method in [53] uses the voltage step of $0.5V_{\text{oc-mod}}$ to scan the P - V curve for GMPP. However, this method may not find GMPP in scanning with step of $0.5V_{\text{oc-mod}}$ in some cases [54].

The R-GMPPT method, which is a modified $0.8V_{\text{oc-mod}}$ model method, is proposed in [55]. In [55], it is stated that for an n PV modules connected in series under nonuniform irradiance conditions, the P - V curve shows n divide intervals, and every interval has one peak power points (PPPs). The voltage and current of the j th ($j = 1, 2, \dots, n$) PPP, i.e., V_{mj} and I_{mj} can be expressed as

$$I_{mj} \approx 0.9I_{scj} \quad (14)$$

$$V_{mj} \approx (j - 1)V_{\text{oc-mod}} + 0.76V_{\text{oc-mod}} = \frac{(j - 1 + 0.76)V_{\text{oc}}}{n} \quad (15)$$

where I_{scj} is the short-circuit current of the j th PV module, V_{oc} and $V_{\text{oc-mod}}$ are the open-circuit voltage of the PV string and module, respectively. A simple PV string is used as an example to make the concept of the above formulas clear, as shown in Fig. 17. As seen, A and B are the PPPs of this string. On the left of point M, only PV1 works, it is well known that the current of PPP A is approximately equal to $0.9I_{sc1}$ (short-circuit current of PV1), and the voltage of PPP A is approximately equal to $0.76V_{oc1}$ (open-circuit voltage of PV1). On the right of point M, PV1 and PV2 works, but the I - V curve is mainly affected by PV2. Thus, the current of PPP B is approximately equal to $0.9I_{sc2}$, and the voltage of PPP B is approximately equal to sum of V_{oc1} and $0.76V_{oc2}$. For simplicity, V_{oc1} and V_{oc2} can be considered equal to $V_{\text{oc-mod}}$, which is equal to half of the open-circuit voltage of the PV string V_{oc} . That is, $V_{m1} = 0.76V_{\text{oc}}/2$ and $V_{m2} = (1 + 0.76)V_{\text{oc}}/2$.

According to (14) and (15), the approximate power of all PPPs can be calculated as

$$P_{mj} \approx V_{mj}I_{mj} \approx \frac{(j - 0.24)V_{\text{oc}}}{n} \cdot 0.9I_{scj}. \quad (16)$$

With the maximum value in these calculated P_{mj} , the neighborhood of GMPP can be determined. Then, the P&O method is used to accurately track the GMPP. As reported in [55], the R-GMPPT method can reduce more than 90% of the tracking time that is consumed by the conventional global searching method, while maintains acceptable tracking accuracy.

Similar to the concept of R-GMPPT method, the proposed I - V curve mapping method in [56] maps out the pattern of I - V curve under nonuniform irradiance conditions by sampling the array current. Based on the analysis of the step-like I - V curve under nonuniform irradiance conditions, it is shown that the

TABLE VII
PERFORMANCE COMPARISON OF DIFFERENT GMPPPT TECHNOLOGIES

Method	Accuracy	Speed	Sensed parameters	Notes
DIRECT [44]	High	Fast	• Voltage and current of PV array	Track the GMPP by gradually reducing the searching range until the GMPP is finally located
Fibonacci [45]	Medium	Medium	• Voltage and current of PV array	
MPT method [46]	High	Fast	• Voltage and current of PV array • Array GMPP current at STC	
I-V curve approximation [47]	High	Fast	• Voltage and current of PV array	
Load-line [48]	Low	Very fast	• Voltage and current of PV array	
Power increment [49]	Very high	Medium	• Voltage and current of PV array	
Ramp voltage scanning [50]	Very high	Medium	• Voltage and current of PV array • Module's open circuit voltage	
$0.8V_{oc-mod}$ model method [51-54]	Relatively high	Relatively Fast	• Voltage and current of PV array	
R-GMPPT [55]	Medium	Very fast	• Voltage and current of PV array • Short circuit current of each module	
I-V curve mapping [56]	High	Fast	• Voltage and current of PV array • Module's open circuit voltage	
Intelligent algorithms [58-60]	Very High	Medium to fast	• Voltage and current is required in most cases	Complex to implement

current in each step of the I - V curve is almost constant up to the end of that step. Moreover, the starting points of each step are in near left-side neighborhood of the multiples of module's open-circuit voltage V_{oc-mod} . According to the above observation, this method samples the array current in multiples of V_{oc-mod} and compares these sampling currents against each other. As a result, the number and length of I - V curve's steps are determined. Then, based on the mapping, the hill climbing algorithm is called to search the vicinity of the multiples of $0.8 V_{oc-mod}$ to track all MPPs. Finally, by comparing the value of tracked MPPs, GMPP is determined. A similar method is proposed in [57], this method can map out the locations of all LMPPs by measuring the voltages of every PV modules and calculates the appropriate reference voltage to track the GMPP around it. Obviously, compared with the method in [57], the I - V curve mapping method is simple to implement. Because the I - V curve mapping method only needs just one current sensor to track GMPPT, while the method in [57] uses one current sensor for each PV module.

The third group includes some intelligent algorithms, such as particle swarm optimization [58], artificial bee colony [59], and fuzzy-logic control [60]. The advantages of intelligent algorithms are their adaptive ability of accurately tracking GMPP regardless of the condition of illumination and the configuration of the PV array. However, the intelligent algorithms are complex to implement, and the initial point must be carefully selected by professionals.

The development of GMPPT techniques is more attractive due to simplicity of implementation, reduced cost, and the immediate adoption to existing system. Table VII provides the performance comparison of the GMPPT methods mentioned above. A more detailed review on the GMPPT techniques can be found in [61]. Note that, although it can harvest more energy by utilizing the global MPPT techniques, it has no effect on the power loss caused by the Gaussian beam.

b) *Modified PV receiver geometries:* The second category to maximize the efficiency of the PV array would be employing different modified PV receiver geometries.

In [12], the radial orientation array is proposed, as shown in Fig. 18(a). By placing the PV cells on a radial to the center point of the receiver or adjusting the manufacturing of the cells

to obtain an optimal radial geometry that reflects the Gaussian distribution of the laser beam, an equal average illumination per cell can be achieved for the series-connected PV cells in each annular area. In this way, the uniformity of the junction illumination can be improved. However, the geometrical loss, complicated structure, and high cost are major issues that limit the implementation of the radial orientation array.

On the other hand, a sawtooth-configured array in which the PV cells are angled is proposed in [52], as shown in Fig. 18(b). With the angled PV cells, the irradiance at each point is reduced by a reduction factor. The reduction factor is a function of a cosine of the angle of the incident beam. The closer to the center of the array, the bigger the angle and the more laser power is reflected. Therefore, with this surface geometry arrangement, all cells in the array substantially can receive the same irradiance. However, the reflected laser beam caused by the angle of each cell could significantly reduce the power transfer to the PV cell, and it is an obstacle for the efficiency improvement of the PV receiver.

In [21], a complicated PV receiver, which is named PV cavity converter (PVCC), is proposed. As shown in Fig. 18(c), the PVCC couples the light into the interior of a cavity through a small aperture on the cavity wall without reflection and impinges directly on a near lambertian diffuser. The back-scattered light illuminates the cavity uniformly, so that the effects of the nonuniform irradiance can be avoided. Benefit from photon recycling in the cavity, the PVCC has the potential to convert high density laser to electricity at unprecedented efficiency. However, the current PVCC prototype functioning within the 100 W to 200 W laser power level only has a efficiency of 14%. It has been analytically shown that an array conversion efficiency of over 60% can be achieved if cells with perfectly matching band-gaps are used as well as the flux density inside of the sphere and the cell population density within the PVCC are increased. Its worth pointing out that, at that such small aperture on the cavity, the high pointing accuracy is required.

c) *Array configuration:* An alternate approach is one that employs different PV array configurations for interconnecting PV cells or modules, which are typically either series-parallel (SP), total cross-tied (TCT), or bridge-linked (BL) configura-

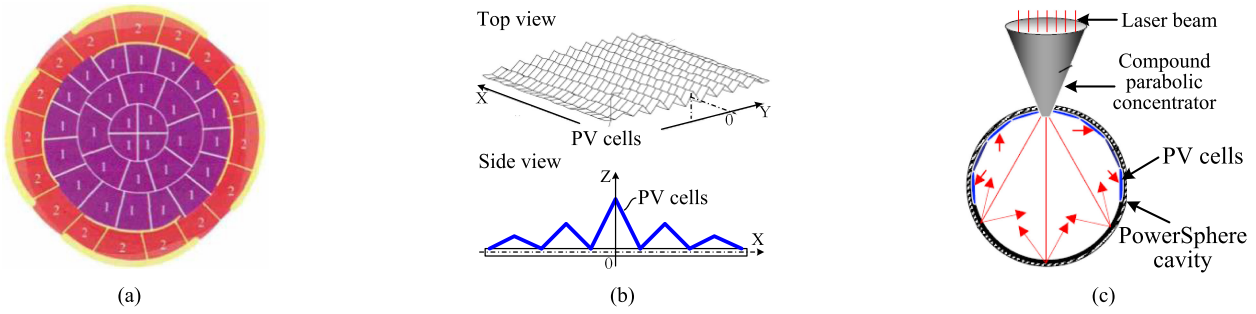


Fig. 18. Different PV receiver geometries to mitigate the effects of the nonuniform irradiance. (a) Radial orientation array. (b) Sawtooth configured array. (c) PV cavity converter.

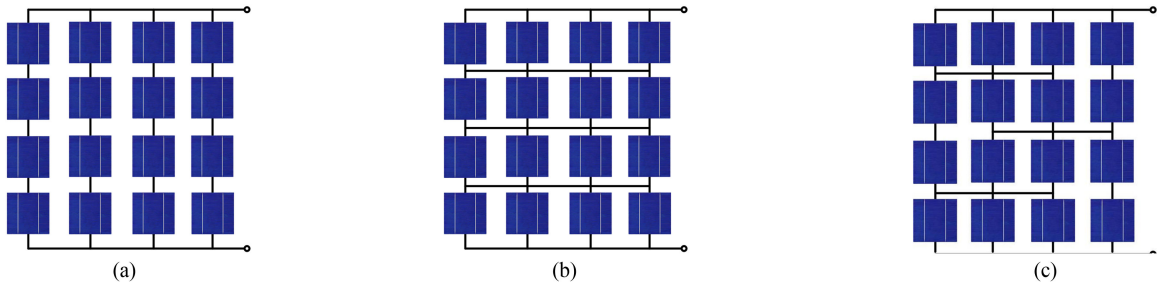


Fig. 19. Different configurations of PV array. (a) SP configuration. (b) TCT configuration. (c) BL configuration.

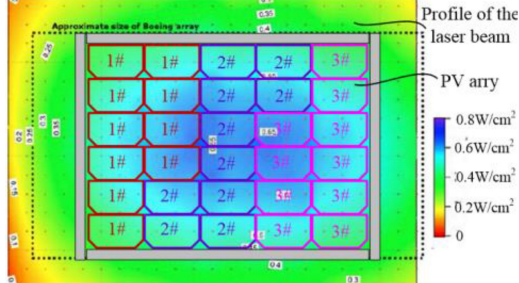


Fig. 20. Measured profile of the laser beam and the schematic of interconnected PV cell in [20].

tions [63], [64], as shown in Fig. 19. Obviously, the actual electrical connections of the PV cells in the PV array are different for different configurations, resulting in different GMPPs under the same Gaussian beam condition. In order to improve the performance of the PV array to counter Gaussian laser beam, the PV array configuration needs appropriate design according to the energy distribution of the laser beam. As the TCT and SP configurations are widely used in practice, thus, these two configurations are discussed here, in order to explore their performance under Gaussian beam condition.

In [20], the SP array is employed and the interconnection scheme is designed to minimize the impact of beam nonuniformity using the energy distribution of the laser beam. Fig. 20 shows the energy distribution of the laser beam and the interconnections design. The color coding is used to show those cells that are connected in series. Thus, the same numbered cells are in series. It can be seen that the irradiances on the PV cells in the same PV string are closed to each other, so that the maxi-

mum power of each string can be maximized to a certain extent. The measured efficiency of this SP array was 21.9% under a laser beam at 0.3 W/cm^2 . However, this was less than half the expected efficiency due to the beam nonuniformity.

In [65], it is found that the interconnections between the PV strings are able to balance the irradiance across each tier in the TCT structure. This may decrease the current that flows through the mismatched cells; thus, blocking the operation of bypass diodes. Therefore, compared with the traditional SP array structure, the TCT structure can improve the MPP of the PV array under nonuniform irradiance conditions. In [66] and [67], the experimental results show that the TCT configuration can improve the amount of maximum power by 5.84% and 3.8% compared with the SP configuration under different nonuniform illumination conditions, respectively. Obviously, for the TCT configuration, swapping the cells from one position to another can obtain different MPPs. For optimal performance, the PV cells in the TCT configuration need to interconnect in an irradiance equalization manner, so that the total irradiance (and therefore current producing ability) at each tier is almost equal.

In many literatures, different reconfigurable PV arrays are proposed to cope with the Gaussian beam condition. For example, a reconfigurable TCT PV array is developed in [68]. As shown in Fig. 21, this reconfigurable array consists of two parts: a large fixed bank of PV array and a small adaptive bank of PV array. The switching matrix, which connects the fixed and adaptive part, is used to recombine the individual PV cells in the array under nonuniform illumination conditions. The switching matrix is controlled by an adaptive reconfiguration algorithm to automatically connect the most illuminated PV cells in the adaptive bank to the least illuminated row of the fixed part, so that each PV module is composed of the PV array operating under

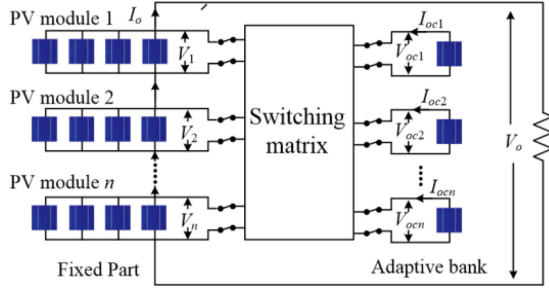
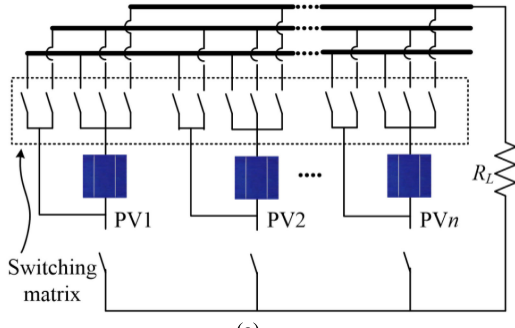
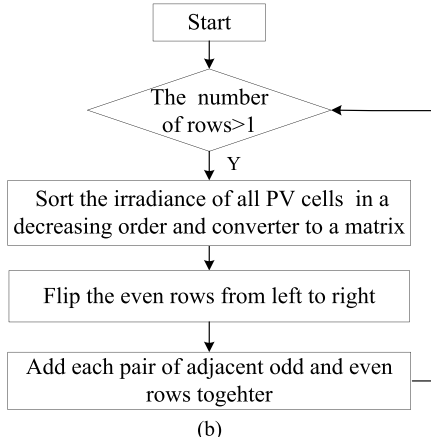


Fig. 21. Reconfigurable PV array proposed in [68].



(a)



(b)

Fig. 22. DPVAs proposed in [68]. (a) Configuration of DPVAs. (b) Algorithm for DPVAs.

similar irradiance conditions. As reported in [68], for a 3×3 TCT PV array with a 3×1 adaptive part, there is a 65% increase in output power from before to after the reconfiguration.

Another reconfigurable PV arrays with TCT configuration, which is named dynamic PV arrays (DPVAs), is developed in [69] to cope with the effects of nonuniform irradiance. As shown in Fig. 22(a), the biggest advantage of the DPVAs is that the dimensions of the PV array can be arbitrary resized and all possible connection schemes are available in practice. As proposed in [69], the best connection scheme of DPVA is determined by the irradiance equalization algorithm. This irradiance equalization algorithm is essentially an iterative and hierarchical sorting algorithm and the flowchart of it is shown in Fig. 22(b). As the irradiance equalization algorithm is based on simple sorting, flipping and adding, the searching time of it is very fast, which means the algorithm is suitable for large PV array. As reported in [69], the DPVAs can achieve over 10% improvement in efficiency than a conventional static array.

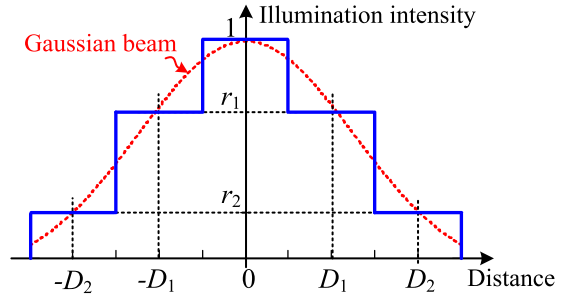


Fig. 23. Simplified model of Gaussian beam.

As given above, the reconfigurable PV array shows the most improvement of MPP compared with the static TCT configurations under the frequently changing illumination conditions. However, the reconfigurable PV array is complex and not cost efficient. Since the Gaussian distribution of the laser beam is constant and regular, it is considered that there exists a certain optimal interconnection scheme which is able to maximize the PV array output power under Gaussian beam condition. Thus, in the field of LPT technology, finding an appropriate configuration is the most common way to improve the efficiency of the PV array. Furthermore, instead of developing the real-time reconfigurable PV array, it is a good option to employ a fixed configuration for arranging the cells so as to enhance the PV power generation under Gaussian beam condition.

In order to do so, an optimal configuration research algorithm for static TCT configuration is proposed in [70]. Since the output power of a PV array is related to the irradiance value of each PV cell, the irradiance across a PV array under Gaussian beam condition is simplified first in [70]. As seen in Fig. 23, the process of simplifying the energy distribution of Gaussian laser is essentially using a step function to fit the Gaussian function. Then, according to the irradiance on every individual PV cell in the TCT array under Gaussian laser beam condition, the optimal TCT configuration search algorithm based on the irradiance equalization method is proposed. The main steps of this algorithm are summarized as follows.

First, define and sort the irradiance of all the PV cells in the PV array in a decreasing order and converted to a PV cell bank. Then, connect the most illuminated PV cell in the PV cell bank in parallel to the module which has the smallest total irradiance. This process will continue until all the PV cells which in the PV cell bank are connected parallel to the rows of the TCT configuration.

As reported in [70], the simulation results show that there is a 33% increase in the MPP power from before to after the algorithm is executed for the 3×3 TCT PV array. Moreover, the experimental results indicate that the optimal 3×3 TCT configuration has better performance than the optimal 3×3 SP configuration with a 9.2% improvement in the MPP power.

d) Power electronics equalizer: In fact, the partial shading effects in the PV arrays have been widely investigated, and the effect of Gaussian beam condition for PV array is a special case of that. Thus, the concept of the power electronics equalizer used to mitigate the partial shading effects can be borrowed to further enhance the output power of PV arrays under the Gaussian beam condition. The aim of the power electronics equalizer is

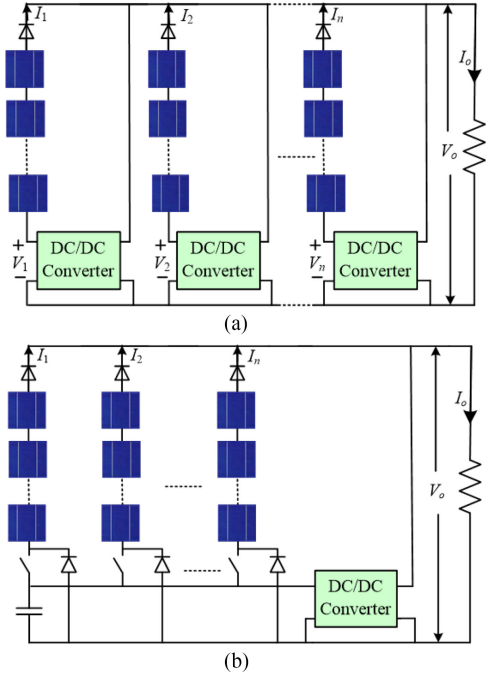


Fig. 24. Voltage injection topology. (a) Voltage injection circuit proposed in [71]. (b) Voltage injection circuit proposed in [72].

to eliminate the multiple peaks, so that only one PPP exhibited in the P - V curve under Gaussian beam condition. In general, the circuit topologies of the power electronics equalizer differ in their implementation, efficiency, number of active and passive elements, complexity of control systems, upgradability, and the capability of individual MPPT for each PV module. Here, three different groups are discussed.

The first group, which is named voltage injection topology [71], [72], is shown in Fig. 24. In Fig. 24, every single PV string is series connected with a dc–dc converter. The main function of the dc–dc converter is to provide the bias voltage $V_{bias,i}$ for the i th PV string, so that the GMPP of the less illuminated string can be aligned with the MPP of the highest illuminated string, resulting in more power can be extracted from the PV array, as illustrated in Fig. 25. This circuit topology can be upgraded by using more dc–dc converters as the number of PV strings increases. However, the additional circuits increase the system complexity and cost.

The second group is the compensation circuits that are employed to improve the output power of a PV string by controlling the voltages of PV modules at its MPPs. Here, two different approaches are discussed.

In the first approach, the generation control circuit (GCC), which is based on the multichopper topology is proposed in [73], as shown in Fig. 26. In this topology, each unit is controlled to regulate its output voltage to ensure that all the PV modules are working at their MPPs by adjusting the off-duty ratio of its switch. Although this topology has good performance in improving the output power of a PV string and can be upgraded as the number of PV modules increases, its implementation is complex for long PV string. It should be noted that the GCC scheme only makes the PV modules operate at an approximate MPP based on the assumption that the MPP voltage

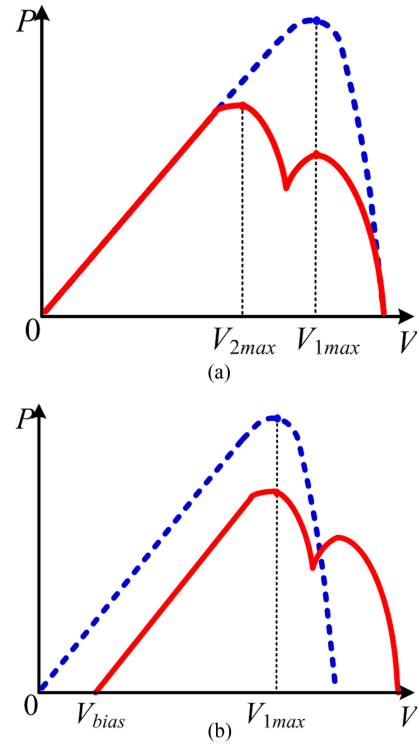


Fig. 25. Effect of bias voltage on the PV string P - V curves. (a) Without bias voltage injection. (b) With bias voltage injection.

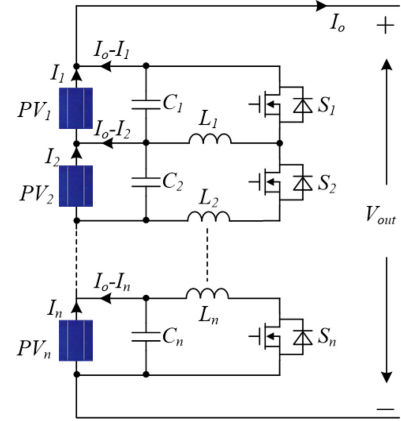


Fig. 26. Multichopper-based GCC.

does not change significantly with irradiation and/or temperature. However, the MPP voltage does change with irradiation and temperature.

Therefore, in the second approach, a more accurate compensation scheme is proposed in [74], referred to here as two mode compensation scheme. In this scheme, a flyback converter is connected parallel to each PV module, as shown in Fig. 27. Here, the flyback converter can operate in two modes: resonant MPPT mode and normal flyback mode. First, in order to determine the MPP voltage of each module, the flyback converter is controlled to operate in a resonant MPPT mode, so that the voltage of PV module begins to resonate and passes through the MPP voltage. Then, the flyback converter is controlled to

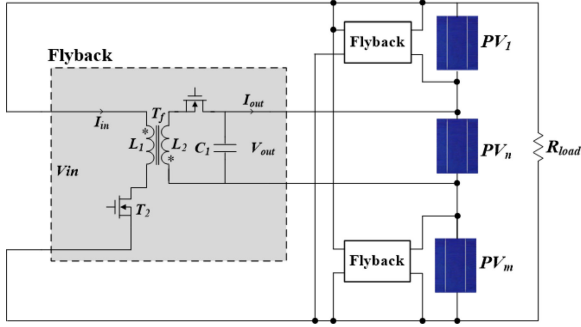


Fig. 27. Topology of two mode compensation scheme.

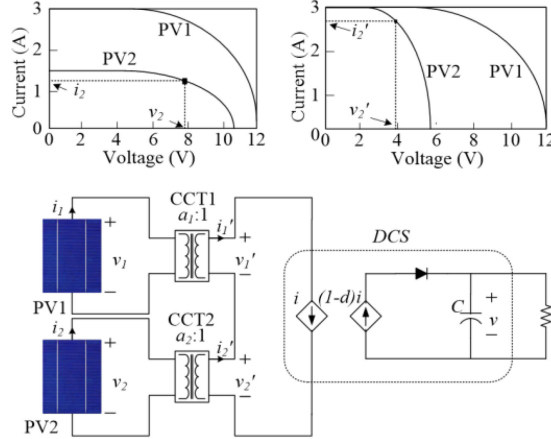


Fig. 28. Topology of CCT.

operate in normal flyback mode to regulate the PV module's voltage at its desired MPP value. In [74], the experimental results show that the two mode compensation scheme can improve the amount of maximum power by 14.6% compared with the GCC scheme.

In the third group, several topologies based on current compensation are proposed. The output current of these circuits is used to compensate the difference between the string current and the current of the less illuminated PV module. Here, three typical types of these circuits are reviewed.

In [75], the returned energy current converter (RECC), referred to here as Type I, is introduced. The RECC unit is controlled as a current source to inject the correct magnitude of current into the PV terminal and consequently balance the current in the PV string. The power associated with the injection of the compensation current is taken from the output of the string. However, the desired current level in the PV string remains to be determined for the power circuit loss minimization.

In type II, the controllable current transformer (CCT) is proposed, as shown in Fig. 28 [76]. As seen, each CCT unit is paralleled with a PV module, and the output terminals of these units are connected in series. Any degree of decline in the output current of less illuminated PV module (PV2) would activate the corresponding CCT (CCT2) to magnify the output current (i'_2) in order to match the PV string current (i'_1). To consider minimizing the power circuit loss, the CCT output current is controlled at an appropriate value by a dependent current source. Although accuracy of this method is high and it can decrease the effect of

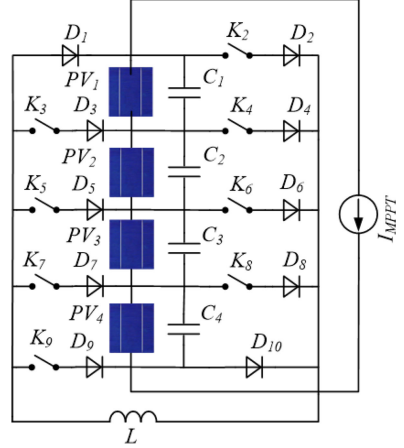


Fig. 29. Topology of PV equalizer.

nonuniform irradiance conditions on the array power, its implementation is expensive.

In type III, a PV equalizer, which is based on the battery voltage equalization circuit, is proposed in [77]. Its topology is shown in Fig. 29. As seen, the equalizer is much simpler due to its single inductor compared with types I and II. The equalizer has three modes: equalize, bypass, and search. The equalize mode is the main function of the equalizer. It draws the excess current from the most illuminated module groups and shares it with the shaded ones. This is done through the successive charging and discharging of an inductor at high frequency by choosing the appropriate switches to be controlled and their duty cycle.

Table VIII provides an overview of the advantages and disadvantages of different compensation circuits that are discussed above. Above all, Table IX provides an overview of the key advantages and potential disadvantages of different approaches that specifically mitigate the Gaussian beam effects. It can be seen that the efficiency of the PV array can be improved by using different modified MPPT methods and employing different PV array configurations.

IV. OPEN RESEARCH ISSUES

A. Efficiency Improvement Issue

As the technology evolves, the possibility of the HILPB system applications is becoming an increasing reality. But the overall system efficiency is currently around 10%–20%, which is a big barrier to the commercial development of the system. Research will continue in the improvement of system efficiency for practical applications. The primary area for efficiency improvement is PV cells. However, most research on the PV cell has been aimed at improving the efficiency for solar cells, which must convert broad-spectrum light. Efforts to optimize “laser” cells suitable for power beaming have been limited. A “laser cell” development effort similar to the DARPA SHEDS program that succeeded in improving the efficiency of LD up to 85% should be done.

B. Safety Issues

As the word “laser” conjures up the idea of a death ray to many, the power density used in the wireless power systems

TABLE VIII
COMPARISON TABLE FOR DIFFERENT POWER ELECTRONICS EQUALIZER

Method	Key advantages	Potential disadvantages
Voltage injection based topology [71-72]	<ul style="list-style-type: none"> ● Simple to implement ● Upgradability 	<ul style="list-style-type: none"> ● The system complexity and cost increase with increase in the number of modules
Multi-chopper based GCC [73]	<ul style="list-style-type: none"> ● PV modules operate at an approximate MPP ● Upgradability 	<ul style="list-style-type: none"> ● Complicated control structure
Two mode compensation scheme [74]	<ul style="list-style-type: none"> ● Attainable theoretical GMPP by providing an accurate compensation ● Upgradability 	<ul style="list-style-type: none"> ● Large number of voltage and current sensor is required ● Disconnection of the PV array from the load during the resonant MPPT mode
RECC [75]	<ul style="list-style-type: none"> ● Control scheme remains simple even with large number of PV module in a string ● Upgradability 	<ul style="list-style-type: none"> ● The desired current level in the PV string remains to be determined for the power circuit loss minimization.
CCT [76]	<ul style="list-style-type: none"> ● Current sensors for each module can be eliminated ● Attainable theoretical GMPP with consideration of circuit loss ● Upgradability 	<ul style="list-style-type: none"> ● Complex architecture and control method
PV equalizer [77]	<ul style="list-style-type: none"> ● Simple architecture ● Upgradability 	<ul style="list-style-type: none"> ● Control complexity increase with increase in the number of modules

TABLE IX
COMPARISON TABLE FOR SOME POSSIBLE APPROACHES THAT MITIGATE THE GAUSSIAN BEAM EFFECTS

Type	Key advantages	Potential disadvantages
Global MPPT technologies	<ul style="list-style-type: none"> ● Simplicity of implementation ● Low cost ● Immediate adoption to existing system ● Improve efficiency to a certain extent 	<ul style="list-style-type: none"> ● No effect on the power loss caused by the Gaussian beam
Modified PV receiver geometries	<ul style="list-style-type: none"> ● Mitigate Gaussian beam effects in PV arrays to a certain extent 	<ul style="list-style-type: none"> ● Geometrical loss ● High cost ● Limited efficiency improvement
Array configuration	<ul style="list-style-type: none"> ● Simplicity of implementation ● Low cost ● Mitigate Gaussian beam effects in PV arrays in theory ● Acceptable efficiency improvement 	<ul style="list-style-type: none"> ● Cells arrangement is complicated ● Practical efficiency usually less than the expected efficiency
Power electronics equalizer	<ul style="list-style-type: none"> ● Mitigate Gaussian beam effects in PV arrays ● MPPT for individual PV modules ● High energy harvest efficiency 	<ul style="list-style-type: none"> ● Complex PV system and control structure ● High cost

would be too high to burn anything that passes through the laser beam, such as vehicles, planes, or birds, if kilowatt and higher power laser beams are to be used. Thus, there is a need for a safety system, like the scanning LIDAR, to shut off the system as soon as an animal or aircraft approaches the beam, and then quickly reacquire the target when it is clear.

Furthermore, the most efficient lasers, e.g., LD, operate at near-infrared wavelengths that are in the retinal hazard region, beyond what ordinary human vision can see. Therefore, special precautions need to be taken to eliminate eye hazards. Longer wavelength light outside the retinal hazard region could be a better solution because it is not focused by the eye. However, such “eye-safe” power beaming systems have lower efficiency and much higher cost. As the laser technology gets improved in the future, more-efficient long-wavelength systems will be available for power beaming.

C. Optical Communications With Laser Power Issues

Future HIPBL system will most likely consist of combination of optical communication technology that operates efficiently together. By utilizing the PV cells as a detector for communications, forward command and control information may be send

concurrently with the power transmission, resulting in a dual use system. The ability to incorporate communications signal into the optical energy delivery path offers an opportunity for the development of the robust free space optical communication system. However, how to effectively modulate information signals onto the transmitted high-intensity photonic energy is still an open problem.

D. Power Management for the HILPB System Based on Maximum Efficiency Identification

As was previously discussed, driving LD in a pulse mode offers the advantage of high efficiency. By pulsing the laser, the entire HILPB system may be abstractly modeled as an optically coupled switched-mode dc/dc converter as shown in Fig. 30.

In order to exploit the best performances of the HILPB system, the relationship of operating conditions, such as switching frequency, duty cycle, and the irradiance of the cells, with maximum efficiency points of the HILPB system should be evaluated. Thus, developing a power management to maximize the system efficiency and balance the power between the generated and demand powers should be considered in the future.

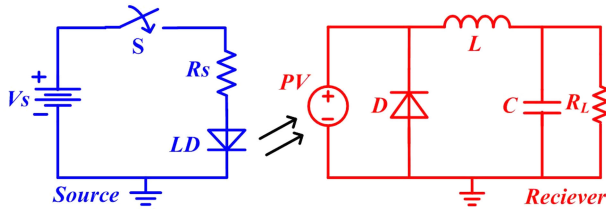


Fig. 30. Optically coupled switched-mode dc/dc converter abstraction for the HILPB system.

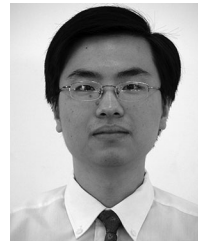
V. CONCLUSION

In this paper, the state-of-the-art in LPT technology is reviewed. The recent progress on laser WPT is described. Several available types of lasers and PV cells are presented. The use of commercially available LD and GaAs PV cell proved to be effective. Current laser technology and reasonable apertures can produce useful beam intensity at the receiver within a range of 10 km. In the operation of the HILPB system, it can be seen that the power system met with barriers arising from beam nonuniformity, which hinder the improvement of the system efficiency and may overcome through the use of modified MPPT methods and different PV array configurations. Moreover, the performance of the LD that operates in a pulsed mode is presented, which has advantages in efficiency. Therefore, it may offer a chance to improve the operation efficiency of the system. Additionally, the open issues and challenges for future research are provided. Further research in laser WPT requires the combined efforts of the professionals and researchers in the areas of PE, control, laser, material science, and optical. The major challenge for the future is further improvements in laser WPT with better energy efficiency for a given transmission distance.

REFERENCES

- [1] S. Y. R. Hui, W. Zhong, and C. K. Lee, "A critical review of recent progress in mid-range wireless power transfer," *IEEE Trans. Power Electron.*, vol. 29, no. 9, pp. 4500–4511, Sep. 2014.
- [2] X. Lu *et al.*, "Wireless charging technologies: Fundamentals standards, and network applications," *IEEE Commun. Surv. Tuts.*, vol. 18, no. 2, pp. 1413–1452, Apr.–Jun. 2016.
- [3] F. Lu, H. Zhang, H. Hofmann, and C. Mi, "A double-sided LCLC compensated capacitive power transfer system for electric vehicle charging," *IEEE Trans. Power Electron.*, vol. 30, no. 11, pp. 6011–6014, Nov. 2015.
- [4] C. Park, S. Lee, G. Cho, and C. Rim, "Innovative 5m-off-distance inductive power transfer systems with optimally shaped dipole coils," *IEEE Trans. Power Electron.*, vol. 30, no. 2, pp. 817–827, Feb. 2015.
- [5] B. Choi, E. Lee, J. Huh, and C. Rim, "Lumped impedance transformers for compact and robust coupled magnetic resonance systems," *IEEE Trans. Power Electron.*, vol. 30, no. 11, pp. 6046–6056, Nov. 2015.
- [6] B. Strassner and K. Chang, "Microwave power transmission: Historical milestones and system components," *Proc. IEEE*, vol. 101, no. 6, pp. 1379–1396, Jun. 2013.
- [7] Q. Liu *et al.*, "Charging unplugged: Will distributed laser charging for mobile wireless power transfer work," *IEEE Veh. Technol. Mag.*, vol. 11, no. 4, pp. 36–45, Dec. 2016.
- [8] S. Kim and J. T. Boys, "Tripolar pad for inductive power transfer systems for EV charging," *IEEE Trans. Power Electron.*, vol. 32, no. 7, pp. 5045–5057, Jul. 2017.
- [9] S. Li and C. Mi, "Wireless power transfer for electric vehicle applications," *IEEE J. Emerg. Sel. Topics Power Electron.*, vol. 3, no. 1, pp. 4–17, Mar. 2015.
- [10] D. E. Raible, "High intensity laser power beaming for wireless power transmission," Master's Thesis, Dept. Elect. Comput. Eng., Cleveland State University, Cleveland, OH, USA, May 2008.
- [11] N. Kawashima and K. Takeda, "Laser energy transmission for a wireless energy supply to robots," in *Proc. Symp. Automat. Robot. Construction*, 2005, pp. 373–380.
- [12] D. Shi *et al.*, "Research on wireless power transmission system between satellites," in *Proc. IEEE Wireless Power Transfer Conf.*, 2016, pp. 1–4.
- [13] D. E. Raible, "Free space optical communications with high intensity laser power beaming," Doctor's Thesis, Dept. Elect. Comput. Eng., Cleveland State Univ., Cleveland, OH, USA, Jun. 2011.
- [14] W. S. Jones, L. L. Morgan, J. B. Forsyth, and J. P. Skratt, "Laser power conversion system analysis, volume 2," *Lockheed Missiles Space Corp.*, Palo Alto, CA, USA, 1979.
- [15] F. Steinsiek *et al.*, "Wireless power transmission experiment as an early contribution to planetary exploration missions," in *Proc. Int. Astronaut. Congr.*, 2003, pp. 169–176.
- [16] E. B. Daniel *et al.*, "Photovoltaic concentrator based power beaming for space elevator application," in *Proc. AIP Conf.*, 2010, pp. 271–182.
- [17] "AUVSI: LaserMotive, Lockheed demonstrate real-world laser power," 2012. [Online]. <https://www.flightglobal.com/news/articles/auvsi-lasermotive-lockheed-demonstrate-real-world-laser-375166/>
- [18] T. He *et al.*, "High-power high-efficiency laser power transmission at 100m using optimized multi-cell GaAs converter," *Chin. Phys. Lett.*, vol. 31, no. 10, pp. 1042031–1042035, 2014.
- [19] "Laser power: Russia develops energy beam for satellite refueling," 2015. [Online]. http://www.spacedaily.com/reports/Laser_Power_Russia_develops_energy_beam_for_satellite_refueling_999.html
- [20] M. D. Smith and H. W. Brandhorst, "Support to a wireless power system design," *Air Force Res. Lab.*, OH, USA, 2011.
- [21] U. Ortabasi and H. Friedman, "Powersphere: A photovoltaic cavity converter for wireless power transmission using high power lasers," in *Proc. IEEE Photovolt. Energy*, 2006, pp. 126–129.
- [22] L. Summerer and O. Purcell, "Concepts for wireless energy transmission via laser," Technical Report, *Eur. Space Agency - Adv. Concepts Team*, 2009.
- [23] A. Hertzberg, W. H. Christiansen, E. W. Johnston, and H. G. Alstrom, "Photon generators and engines for laser power transmission," *AIAA J.*, vol. 10, no. 5988, pp. 394–400, 2015.
- [24] K. J. Duncan, "Laser based power transmission: component selection and laser hazard analysis," in *Proc. PELS Workshop Emerg. Technol., Wireless Power Transfer*, 2016, pp. 100–103.
- [25] T. Blackwell, "Recent demonstrations of Laser power beaming at DFRC and MSFC," *Beamed Energy Propul.*, vol. 766, pp. 73–85, 2005.
- [26] J. Mukehrjee, S. Jarvis, M. Perren, and S. J. Sweeney, "Efficiency limits of laser power converters for optical power transfer applications," *J. Phys. D, Appl. Phys.*, vol. 46, no. 26, pp. 6–11, 2013.
- [27] R. Mason, "Feasibility of laser power transmission to a high-altitude unmanned aerial vehicle," RAND Corporation, Santa Monica, CA, USA, Tech. Rep. TR-898-AF, 2011.
- [28] O. Hohn, A. W. Walker, A. W. Bett, and H. Helmers, "Optimal laser wavelength for efficient power converter operation over temperature," *Appl. Phys. Lett.*, vol. 108, no. 24, pp. 971–974, 2016.
- [29] A. W. Bett *et al.*, "III–V solar cells under monochromatic illumination," in *Proc. 33rd IEEE Photovolt. Spec. Conf.*, 2008, pp. 1–5.
- [30] J. Schubert *et al.*, "High-voltage GaAs photovoltaic laser power converters," *IEEE Trans Electron Dev.*, vol. 56, no. 2, pp. 170–175, Feb. 2009.
- [31] C. E. Valdivia *et al.*, "Five-volt vertically-stacked, single-cell GaAs photonic power converter," *Proc. SPIE*, vol. 9358, pp. 93580E-1–93580E-8, 2015.
- [32] E. C. Boris *et al.*, "Remote electric power transfer between spacecrafts by infrared beamed energy," in *Proc. AIP Conf.*, 2011, vol. 1402, pp. 489–496.
- [33] C. A. Schafer, "Continuous adaptive beam pointing and tracking for laser power transmission," *Opt. Express*, vol. 18, no. 13, pp. 13451–13467, 2010.
- [34] Encyclopedia of Laser Physics and Technology-Laser Diodes, 2018. [Online]. Available: http://www.rp-photonics.com/laser_diodes.html
- [35] "Laser power beaming fact sheet," Laser Motive Inc., Kent, WA, USA, 2012.
- [36] W. Zhou and K. Jin, "Efficiency evaluation of laser diode in different driving modes for wireless power transmission," *IEEE Trans. Power Electron.*, vol. 30, no. 11, pp. 6237–6244, Nov. 2015.
- [37] A. Sharma *et al.*, "High power pulsed current laser diode driver," in *Proc. Int. Conf. Elect. Power Energy Syst.*, 2016, pp. 120–126.
- [38] C. J. Dong and H. Huang, "Analysis and design of high-current constant-current driver for laser diode bar," in *Proc. Int. Conf. Electron.*, 2011, pp. 1321–1324.

- [39] I. D. Crawford, "Low noise current source driver for laser diodes," U.S. PatentUS20030062881A1, 2003.
- [40] N. K. Poon *et al.*, "Techniques for input ripple current cancellation: Classification and implementation," *IEEE Trans. Power Electron.*, vol. 15, no. 6, pp. 1144–1152, Nov. 2000.
- [41] M. T. Thompson and M. F. Schlecht, "High power laser diode driver based on power converter technology," *IEEE Trans. Power Electron.*, vol. 12, no. 1, pp. 46–52, Jan. 1997.
- [42] A. Sharma, C. B. Panwar, and R. Arya, "High power pulsed current laser diode driver," in *Proc. Int. Conf. Elect. Power Energy Syst.*, 2016, pp. 120–126.
- [43] G. A. Landis, "Maximum power point tracking scheme for PV systems operating under partially shaded conditions," *J. Propulsion Power*, vol. 9, no. 1, pp. 1494–1502, 2012.
- [44] T. L. Nguyen and K. S. Low, "A global maximum power point tracking scheme employing DIRECT search algorithm for photovoltaic systems," *IEEE Trans. Ind. Electron.*, vol. 57, no. 10, pp. 3456–3467, Oct. 2010.
- [45] N. A. Ahmed and M. Miyatake, "A novel maximum power point tracking for photovoltaic applications under partially shaded insolation conditions," *Elect. Power Syst. Res.*, vol. 78, no. 5, pp. 777–784, 2008.
- [46] A. M. S. Furtado, F. Bradaschia, M. C. Cavalcanti, and L. R. Limongi, "A reduced voltage range global maximum power point tracking algorithm for photovoltaic systems under partial shading conditions," *IEEE Trans. Ind. Electron.*, vol. 65, no. 4, pp. 3252–3262, Apr. 2018.
- [47] M. A. Ghasemi, A. Ramyar, and H. Iman-Eini, "MPPT method for PV system under partially shaded conditions by approximating I - V curve," *IEEE Trans. Ind. Electron.*, vol. 65, no. 5, pp. 3966–3975, May 2018.
- [48] K. Kobayashi, I. Takano, and Y. Sawada, "A study of a two stage maximum power point tracking control of a photovoltaic system under partially shaded insolation conditions," *Solar Energy Mater. Solar Cells*, vol. 90, pp. 2975–2988, Nov. 2006.
- [49] E. Koutroulis and F. Blaabjerg, "A new technique for tracking the global maximum power point of PV arrays operating under partial-shading conditions," *IEEE J. Photovolt.*, vol. 2, no. 2, pp. 184–190, Apr. 2012.
- [50] M. A. Ghasemi, H. M. Foroushani, and M. Parniani, "Partial shading detection and smooth maximum power point tracking of PV arrays under PSC," *IEEE Trans. Power Electron.*, vol. 31, no. 9, pp. 6281–6292, Sep. 2016.
- [51] H. Patel and V. Agarwal, "Maximum power point tracking scheme for PV systems operating under partially shaded conditions," *IEEE Trans. Ind. Electron.*, vol. 55, no. 4, pp. 1689–1698, Apr. 2008.
- [52] J. Ahmed and Z. Salam, "An improved method to predict the position of maximum power point during partial shading for PV arrays," *IEEE Trans. Ind. Informat.*, vol. 11, no. 6, pp. 1378–1387, Dec. 2015.
- [53] M. Boztepe, F. Guinjoan, G. Velasco-Quesada, S. Silvestre, A. Chouder, and E. Karatepe, "Global MPPT scheme for photovoltaic string inverters based on restricted voltage window search algorithm," *IEEE Trans. Ind. Electron.*, vol. 61, no. 7, pp. 3302–3312, Jul. 2014.
- [54] A. Kouchaki, H. Iman-Eini, and B. Asaei, "A new maximum power point tracking strategy for PV arrays under uniform and non-uniform insolation conditions," *Solar Energy*, vol. 91, pp. 221–232, 2013.
- [55] Y. P. Wang, Y. Li, and X. B. Ruan, "High accuracy and fast speed MPPT methods for PV string under partially shaded conditions," *IEEE Trans. Power Electron.*, vol. 63, no. 1, pp. 235–245, Jan. 2016.
- [56] A. Ramyar, H. Iman-Eini, and S. Farhangi, "Global maximum power point tracking method for photovoltaic arrays under partial shading conditions," *IEEE Trans. Ind. Electron.*, vol. 64, no. 4, pp. 2855–2864, Apr. 2017.
- [57] K. Chen, S. Tian, Y. Cheng, and L. Bai, "An improved MPPT controller for photovoltaic system under partial shading condition," *IEEE Trans. Sustain. Energy*, vol. 5, no. 3, pp. 978–985, Jul. 2014.
- [58] A. Koad, A. F. Zobaa, and A. E. Shahat, "A novel MPPT algorithm based on particle swarm optimization for photovoltaic systems," *IEEE Trans. Energy Convers.*, vol. 8, no. 2, pp. 468–476, Apr. 2017.
- [59] K. Sundareswaran *et al.*, "Enhanced energy output from a PV system under partial shaded conditions through artificial bee colony," *IEEE Trans. Sustain. Energy*, vol. 6, no. 1, pp. 198–209, Jan. 2015.
- [60] B. N. Alajmi, K. H. Ahmed, S. J. Finney, and B. W. Williams, "A maximum power point tracking technique for partially shaded photovoltaic systems in microgrids," *IEEE Trans. Ind. Electron.*, vol. 60, no. 4, pp. 1596–1606, Apr. 2013.
- [61] A. Bidram, A. Davoudi, and R. S. Balog, "Control and circuit techniques to mitigate partial shading effects in photovoltaic arrays," *IEEE J. Photovolt.*, vol. 2, no. 4, pp. 532–546, Oct. 2012.
- [62] J. T. Brain, "Photovoltaic receiver for beam power," U.S. Patent 8736712B2, May 27, 2014.
- [63] P. S. Rao, G. S. Ilango, and C. Nagamani, "Maximum power from PV arrays using a fixed configuration under different shading conditions," *IEEE J. Photovolt.*, vol. 4, no. 2, pp. 679–686, Mar. 2014.
- [64] L. Gao, R. A. Dougal, S. Liu, and A. P. Iotova, "Parallel-connected solar PV system to address partial and rapidly fluctuating shadow conditions," *IEEE Trans. Ind. Electron.*, vol. 56, no. 5, pp. 1548–1556, May 2009.
- [65] L. Villa, D. Picault, B. Raison, S. Bacha, and A. Labonne, "Maximizing the power output of partially shaded photovoltaic plants through optimization of the interconnections among its modules," *IEEE J. Photovolt.*, vol. 2, no. 2, pp. 154–163, Apr. 2012.
- [66] M. Jazayeri, S. Uysal, and K. Jazayeri, "A comparative study on different photovoltaic array topologies under partial shading conditions," in *Proc. IEEE PES T&D Conf.*, 2014, pp. 1–5.
- [67] D. Picault, B. Raison, S. Bacha, J. Aguilera, and J. De La Casa, "Changing photovoltaic array interconnections to reduce mismatch losses: A case study," in *Proc. 9th Int. Conf. Environ. Electr. Eng.*, 2010, pp. 37–40.
- [68] D. Nguyen, and B. Lehman, "An adaptive solar photovoltaic array using model-based reconfiguration algorithm," *IEEE Trans. Ind. Electron.*, vol. 55, no. 7, pp. 2644–2654, Jul. 2008.
- [69] J. P. Storey, P. R. Wilson, and D. Bagnall, "Improved optimization strategy for irradiance equalization in dynamic photovoltaic arrays," *IEEE Trans. Power Electron.*, vol. 28, no. 6, pp. 2946–2956, Jun. 2013.
- [70] W. Zhou and K. Jin, "Optimal photovoltaic array configuration under Gaussian laser beam condition for wireless power transmission," *IEEE Trans. Power Electron.*, vol. 32, no. 5, pp. 3662–3672, May 2017.
- [71] E. Karatepe, T. Hiyma, M. Boztepe, and M. Colak, "Power controller design for photovoltaic generation system under partially shaded insolation conditions," in *Proc. Intell. Syst. Appl. Power Syst.*, 2007, pp. 1–6.
- [72] T. Mishima and T. Ohnishi, "A power compensation and control system for a partially shaded PV array," *Elect. Eng. Jpn.*, vol. 146, pp. 74–82, 2004.
- [73] T. Shimizu, M. Hirakata, T. Kamezawa, and H. Watanabe, "Generation control circuit for photovoltaic modules," *IEEE Trans. Power Electron.*, vol. 16, no. 3, pp. 293–300, May 2001.
- [74] P. Sharma and V. Agarwal, "Exact maximum power point tracking of grid-connected partially shaded PV source using current compensation concept," *IEEE Trans. Power Electron.*, vol. 29, no. 9, pp. 4684–4692, Sep. 2014.
- [75] Y. Nimni and D. Shmilovitz, "A returned energy architecture for improved photovoltaic systems efficiency," in *Proc. IEEE Int. Symp. Circuits Syst.*, 2010, pp. 2191–2194.
- [76] W. L. Chen and C. T. Tsai, "Optimal balancing control for tracking theoretical global MPP of series PV modules subject to partial shading," *IEEE Trans. Ind. Electron.*, vol. 62, no. 8, pp. 4837–4848, Aug. 2015.
- [77] F. L. Villa, T. P. Ho, J. C. Crebier, and B. Raison, "A power electronics equalizer application for partially shaded photovoltaic modules," *IEEE Trans. Ind. Electron.*, vol. 60, no. 3, pp. 1179–1190, Mar. 2013.



Ke Jin (S'04–M'09) was born in Nanjing, China, in 1978. He received the B.S., M.S., and Ph.D. degrees in electrical engineering from the Nanjing University of Aeronautics and Astronautics, Nanjing, China, in 2000, 2003, and 2006, respectively.

From 2007 to 2008, he was a Postdoctoral Researcher with the Center for Power Electronics Systems, Virginia Polytechnic Institute and State University, Blacksburg. He is currently a Professor with the College of Automation Engineering, NUAA. He has authored more than 50 technical papers published in international journals and conference proceedings. His main research interests include high-frequency soft-switching conversion, low-voltage high-current conversion techniques, and renewable power systems.



Weiyang Zhou was born in Jiangxi, China, in 1989. He received the B.S. and Ph.D. degrees in electrical engineering from the Nanjing University of Aeronautics and Astronautics, Nanjing, China, in 2011, and 2018, respectively. His current research interests include dc–dc conversion and WPT system.